JOURNAL OF THERMOPHYSICS AND HEAT TRANSFER
Vol. 12, No. 4, October–December 1998

Impingement Cooling in Rotating Two-Pass Rectangular Channels

Kumar V. Akella* and Je-Chin Han†
Texas A&M University, College Station, Texas 77843-3123

Impingement cooling was studied on smooth target walls in rotating two-pass rectangular channels with a sharp 180-deg turn. Jets impinged opposite to the direction of rotation in one channel, and in the same direction of rotation in the other channel. Spent air moved in the radially outward direction in the first impingement channel and radially inward in the second impingement channel. Jet Reynolds numbers and rotation numbers varied from 4×10^3 to 1×10^4 and 0 to 0.0133, respectively. Rotation changed the pressure level and distribution, but did not significantly alter the jet velocity distribution in the two-pass impingement channel. However, rotation-induced Coriolis and centrifugal forces decreased the Nusselt number values 20 and 25% in the impingement channels and turn region, respectively. Nusselt number values in the turn region were 60% higher when compared with those in the impingement channels for higher jet-flow rates and over the range of rotation speeds tested.

Nomenclature

A_f = ratio of total area of jets impinging on a copper plate to area of heated copper plate (open area ratio), $n\pi d_j^2/(4A_w)$
A_w = area of a copper plate
D_h = hydraulic diameter of the impingement channel
d_j = diameter of the impinging jet
$F_{c,\mathrm{Cor}}$ = channel crossflow Coriolis force, $\rho\Omega V_c$
F_{cen} = centrifugal force, $\rho\Omega^2 r$
$F_{j,\mathrm{Cor}}$ = jet Coriolis force, $\rho\Omega V_j$
G_c = channel crossflow mass flux, ρV_c
G_j = jet mass flux, ρV_j
g = gravitational acceleration, 9.81 m/s^2
h = regionally averaged heat transfer coefficient on each copper plate
k = thermal conductivity of air (coolant)
L = length of the test model
m_j = jet mass flow rate
Nu = regionally averaged Nusselt number on each copper plate for the rotating test
Nu_{av} = channel-averaged (first or second) Nusselt number for the rotating test
Nu_0 = regionally averaged Nusselt number on each copper plate for the nonrotating test
$Nu_{0,\mathrm{av}}$ = channel-averaged (first or second) Nusselt number for the nonrotating test
n = number of jets impinging on a copper plate
Pr = Prandtl number of air (coolant)
q_{loss} = heat conducted to the test stand from copper plates
q_{total} = total heat input to the copper plates
Re_j = channel-averaged jet Reynolds number, $\rho V_{j,\mathrm{av}} d_j/\mu$
R_m = mean rotating radius of the test model
Ro = channel-averaged jet rotation number, $\Omega d_j/V_{j,\mathrm{av}}$
r = radial location in the supply and impingement channels from the center of rotation
T_b = measured air temperature in impingement channels
T_f = film temperature, $(T_w + T_b)/2.0$
T_j = air (coolant) temperature measured at the inlet of the first supply channel
T_w = regionally averaged copper plate (wall) temperature
$(T_w - T_j)/T_w$ = ratio of wall-to-air temperature difference to wall temperature, R
V_c = channel crossflow velocity
V_j = jet velocity
$V_{j,\mathrm{av}}$ = channel-averaged jet velocity
X = radial location of wall and air temperature measurements in the impingement channels from the inlet of the first impingement channel
X_n = streamwise distance between adjacent jet holes
Y_n = spanwise distance between jet holes
Z_n = distance between the jet plate and copper plates in the impingement channels
μ = dynamic viscosity of air (coolant)
ρ = density of air (coolant)
Ω = rotation speed of test model, rpm

Introduction

RESULTS from impingement heat transfer on nonrotating blades have been reported. Kercher and Tabakoff[1] and Chance[2] studied the influence of jet diameter, jet arrangement, open area ratio, crossflow, jet velocity, and the ratio of wall-to-coolant temperature difference to wall temperature on impingement heat transfer. Florschuetz et al.[3] presented heat transfer values at various channel crossflow mass flux-to-jet mass flux ratios. Van Treuren et al.[4] reported local heat transfer measurements under an in-line array of circular jets with minimum crossflow. Huang et al.[5] measured local heat transfer values by means of a transient liquid crystal technique with different exit flow orientations.

Few studies measured the effects of rotation on impingement cooling. Epstein et al.[6] obtained heat transfer measurements

Presented as Paper 97-2488 at the AIAA 32nd Thermophysics Conference, Atlanta, GA, June 23–25, 1997; received Oct. 2, 1997; revision received April 23, 1998; accepted for publication April 30, 1998.

*Graduate Research Assistant, Department of Mechanical Engineering.

†HTRI Professor, Department of Mechanical Engineering. Associate Fellow AIAA.

from a single row of circular jets in the leading-edge region of an airfoil with radially outward crossflow. Heat transfer values were presented for two model orientations: the jet direction was perpendicular to the direction of rotation and the jet direction was inclined at a 60-deg angle to the direction of rotation. Epstein et al. concluded that rotation decreased the Nusselt number values 25% compared with nonrotating values. Mattern and Hennecke[7] presented local mass transfer measurements by means of a naphthalene sublimation technique for a single row of circular impinging jets on the leading-edge region of an airfoil. Geometric parameters (X_n/d_j and Z_n/d_j) were varied during the experiments. The angle (stagger angle) between the jet direction and direction of rotation also varied (0, 15, 30, 45, 75, and 90 deg). Results showed that rotation reduced heat transfer values between 10 and 40%, according to the stagger angle. Parsons et al.[8] investigated heat transfer characteristics from an in-line array of circular jets in the midchord region of a blade. Nusselt number values were obtained in twin rectangular impingement channels, with jets impinging in the direction of rotation in one impingement channel and jets impinging opposite to the direction of rotation in the other impingement channel. Spent air moved in the radially outward direction in both impingement channels. Parsons et al. concluded that as the rotation number increased, heat transfer values decreased 20% compared with nonrotating values. However, as the ratio of wall-to-coolant temperature difference to wall temperature increased, heat transfer coefficients decreased 10% while other parameters remained constant.

This study presents flow and heat transfer measurements from an in-line array of circular airjets in the midchord region of a rotating blade. Measurements were obtained in two-pass rectangular impingement channels, with the channels connected by a sharp 180-deg turn. Spent air moved radially outward and then radially inward in the first and second impingement channels, respectively. Measurements were obtained with the jets impinging in the direction of rotation and also impinging opposite to the direction of rotation, in both the first and second impingement channels. Also, the geometric parameters, such as d_j, X_n/d_j, Y_n/d_j, Z_n/d_j, A_f, and R_m/d_j of this investigation, are different from those of Parsons et al. This study measured flow and heat transfer values in a simulated rotating gas turbine blade, focusing the effects of Coriolis and centrifugal forces on a new impingement-cooling configuration.

Experimental Apparatus

Figure 1 shows the schematic of the test model. Compressed air regulated across a sharp-edged orifice flow meter, traveled through a rotating union, an aluminum shaft, and a Teflon® pipe with a length-to-diameter ratio of 12. Air then entered the first rectangular cross-sectioned supply channel (9.53 mm × 19.05 mm) with an aspect ratio of 0.5. Air impinged from an array of circular jets on the target wall (copper plates) in the first impingement channel (9.53 mm × 19.05 mm) (Fig. 1). Ten jets impinged on each copper plate in the impingement channels (only two and six jets impinged on the copper plates just upstream and downstream of the turn region, respectively). Spent air moved radially outward and accelerated in the turn region, and then entered the second supply channel. Air impinged from an array of circular jets on the target wall in the second impingement channel (Fig. 1). After impinging on the target wall, the spent air moved radially inward and exited into the laboratory.

Pressure taps inserted in the supply and impingement channels measured pressure distribution and calculated jet velocities at various radial locations in the test model under adiabatic wall conditions. The pressure transducer in the scanivalve unit was calibrated before and after the pressure measurements.

d_j and A_f were fixed at 3.18 mm and 12%, respectively. The streamwise jet spacing-to-jet diameter ratio, X_n/d_j; spanwise jet spacing-to-jet diameter ratio, Y_n/d_j; and the distance between the jet plate and target wall-to-jet diameter ratio, Z_n/d_j, were

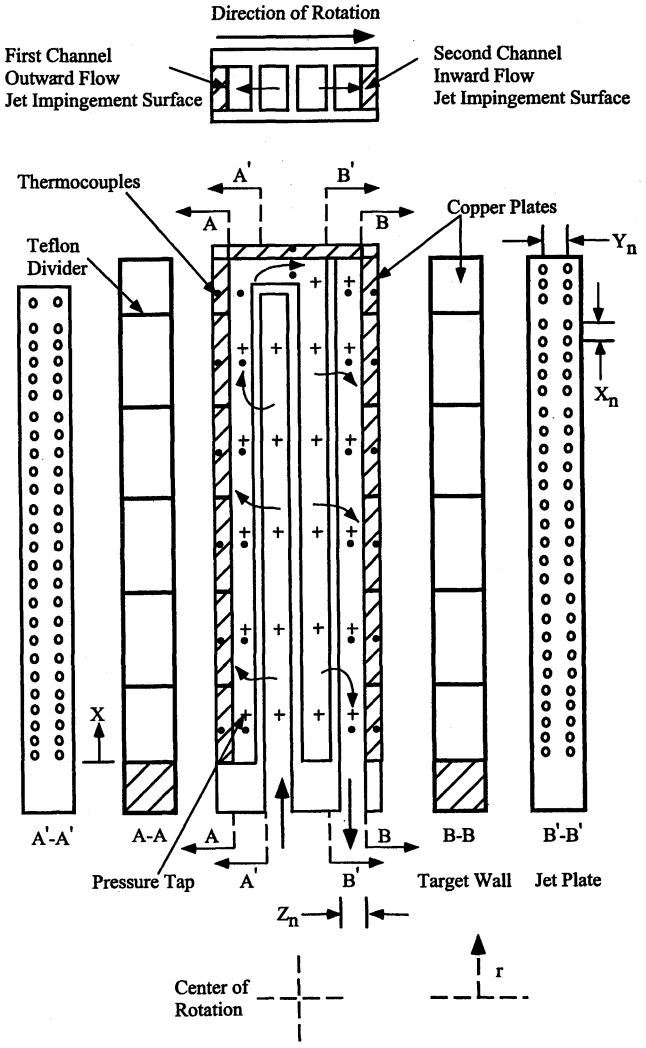

Fig. 1 Schematic of test model.

fixed at 2, 3, and 3, respectively. The thickness of the jet plate-to-jet diameter ratio, t/d_j; mean rotating radius of the test model-to-jet diameter ratio, R_m/d_j; and length of the test model-to-jet diameter ratio, L/d_j, were fixed at 0.5, 197, and 86, respectively.

The target wall in each impingement channel had six copper plates, with dimensions of 34.93 mm × 19.05 mm × 3.18 mm (25.40 mm × 19.05 mm × 3.18 mm for copper plates just upstream and downstream of the turn region). The turn region had one copper plate, with dimensions of 44.45 mm × 19.05 mm × 3.18 mm. The target wall in each impingement channel and the turn region were heated separately by resistance heaters coated with polyester. The heaters were uniformly cemented in the grooves behind the copper plates. This created a nearly uniform wall heat flux boundary condition. Heat conduction to the test stand was minimized by 16-mm-thick Teflon insulation behind the target walls. 1.59-mm-thick Teflon insulation reduced the heat conduction between adjacent copper plates. Thermocouples (T type, copper–constantan) embedded behind the copper plates (six in each impingement channel and one in the turn region) and in the impingement channels measured the regionally averaged wall and air temperatures.

Figure 2 shows the schematic of the rotating impingement test stand. The assembled test model was mounted at one end of the rotating arm with the other end of the arm acting as a counterbalance. A 100-channel slip-ring unit transferred thermocouple readings to the data logger and power to the resistance heaters. A 48-port scanivalve unit was mounted on top of the slip-ring unit for pressure measurement in the test

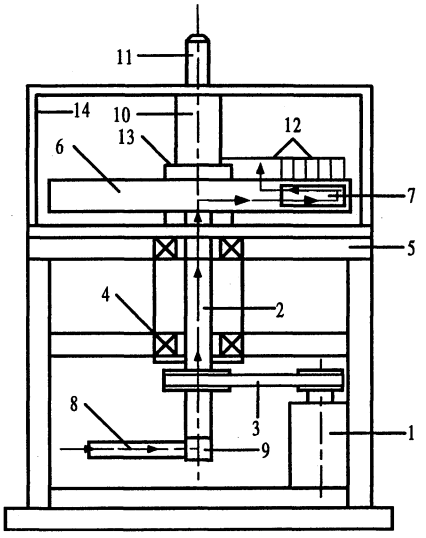

Fig. 2 Schematic of test stand. 1, electric motor, 2, rotating shaft; 3, belt drive; 4, bearing support; 5, steel table; 6, rotating arm; 7, test model; 8, compressed air; 9, rotating union; 10, slip ring unit; 11, scanivalve unit; 12, pressure taps; 13, hub; and 14, safety guard.

model. One additional port was connected to a u-tube manometer for pressure transducer calibration. An electric motor rotated the test model, slip-ring unit, and scanivalve. The instruments to record voltages and currents, transformers, decoder to read pressure transducer signals, and data logger to record thermocouple readings were on a stationary table next to the test stand.

Experimental Procedure and Data Analysis

After the flow rate and rotation speed were achieved, the pressure measurements were made under adiabatic wall conditions. The local jet mass flow rates and jet velocities were calculated from the pressure measurements as shown in Eqs. (1) and (2). S is a constant (0.052), C_d is the channel averaged jet discharge coefficient, P_s is the pressure in the supply channel, P_i is the pressure in the impingement channel, and n is the number of jets impinging on a copper plate at a given radial location. C_d was calculated to be in the range of 0.65–0.67 from the overall mass balance in the test model. The uncertainty in the pressure transducer measurements was ±0.15%, whereas the uncertainties in the calculations of jet mass flow rates and jet velocities were ±2.5 and ±4.0%, respectively.

$$m_j = Sd_j^2 C_d \sqrt{(P_s/T_j)(P_s - P_i)} \tag{1}$$

$$V_j = 4m_j/n\rho_j \pi d_j^2 \tag{2}$$

Heat-loss experiments were performed without air at various temperature levels to account for the heat conducted to the test stand and lost to the surroundings. The heat loss from each copper plate was calculated as shown in Eq. (3). Heat-loss power, q_{loss}, was calculated as a function of temperature difference between the copper plate and the surroundings:

$$q_{\text{loss}} = A + B(T_w - T_{\text{amb}}) \tag{3}$$

A and B are constants evaluated for each copper plate at all of the rotation speeds tested, and T_{amb} is the surrounding (laboratory) air temperature. As rotation speed increased from 0 to 800 rpm at $Re_j = 4 \times 10^3$, the average ratio of heat loss power-to-total power input increased from 0.15 to 0.25. At $Re_j = 1 \times 10^4$, as rotation speed increased, these average ratios increased from 0.10 to 0.17. The heat conduction between adjacent copper plates was less than 2% of the total power input to the copper plates.

The coefficient h was calculated as shown in Eq. (4), where $(q_{\text{total}} - q_{\text{loss}})$ was the net heat entering the copper plates and heating the air (coolant). The bulk air temperatures, T_b, were measured by thermocouples in the impingement channels and the turn region at various radial locations (adjacent to the copper plates). Energy balance was also performed to determine bulk air temperature adjacent to copper plates. Energy balance values were within ±10% of the measurement values for all jet Reynolds numbers and rotation speeds tested. Because the jets and crossflow provide more mixing of the air in the impingement channels, the regionally averaged temperature measurements give a good representation of bulk air temperatures. Therefore, the heat transfer coefficients were calculated based on thermocouple measurements of wall and air temperatures.

$$h = \frac{(q_{\text{total}} - q_{\text{loss}})}{A_w(T_w - T_b)} \tag{4}$$

The uncertainty in the calculation of h depends on the local wall-to-bulk air temperature difference and the net heat input to the air from each copper plate. Based on the method of Kline and McClintock,[9] the uncertainty in the measurement of flow rate entering the supply channel, the channel-averaged jet Reynolds number, and the Nusselt number was estimated at $Re_j = 4 \times 10^3$ were ±6, ±7, and ±10%, respectively. However, these values decreased to ±3, ±4, and ±6%, respectively, at $Re_j = 1 \times 10^4$.

Experimental Results and Discussion

Impingement cooling depends on various parameters: 1) geometry (d_j, X_n/d_j, Y_n/d_j, Z_n/d_j, R_m/d_j, and A_f); 2) flow rate (Re_j); 3) rotation speed (Ro); 4) direction of impingement with respect to rotation direction; 5) direction of channel cross flow; and 6) thermal boundary conditions.

This study was performed for the following conditions: 1) fixed geometric parameters; 2) $Re_j = 4 \times 10^3$, 6×10^3, 8×10^3, and 1×10^4; 3) $\Omega = 0$, 400, and 800 rpm; 4) forward and reverse direction of rotation; 5) radially outward and inward in the first and the second impingement channel, respectively; and 6) uniform wall heat flux boundary condition, or, the ratio of average wall-to-coolant temperature difference to average wall temperature $(T_w - T_j)/T_w = 0.083$ and 0.07 for 0 and 800 rpm, respectively. Target walls were heated up to 52°C (125°F) during the experiments. Operating parameters Re_j and Ω together produced the following jet rotation numbers: Ro = 0.0, 0.0027, 0.0033, 0.0044, 0.0053, 0.0066, 0.0089, and 0.0133. This study measured heat transfer values in a simulated rotating gas turbine blade, focusing the effects of Coriolis and centrifugal forces on a new impingement-cooling configuration. The test model was enlarged, which resulted in larger jet holes and lower jet velocities. Rotation speeds were also lowered. However, the dimensionless parameters, such as Re_j and Ro are in the range of gas turbine operation. Test-channel geometry and jet distribution were arbitrarily selected and not optimized to give the highest heat transfer values from the leading and trailing walls.

Figure 3 shows the pressure distribution in the supply and impingement channels, the jet velocity distribution, and the distribution of the ratio of channel crossflow mass flux-to-jet flow mass flux for the nonrotating test. Higher jet Reynolds numbers resulted in higher pressure levels and higher jet velocities in the test model.

Marching from the inlet to the exit, the pressure in the supply channel increased while the pressure in the impingement channel decreased. This trend indicated that the velocity of air in the supply channel decreased (air velocity goes to zero at the exit) and the velocity of crossflow in the impingement channel increased (crossflow velocity reached maximum at the exit). The jet velocities and ratios of channel crossflow mass

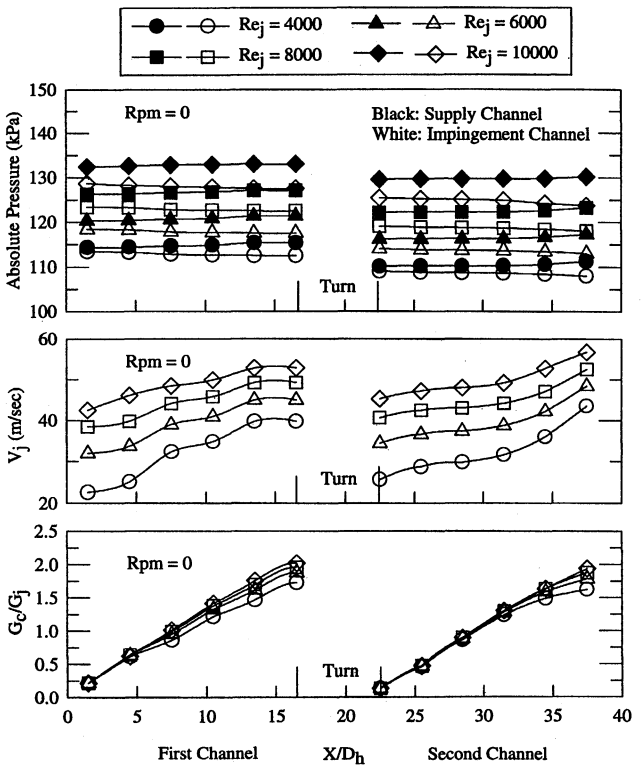

Fig. 3 Flow distribution for nonrotating test.

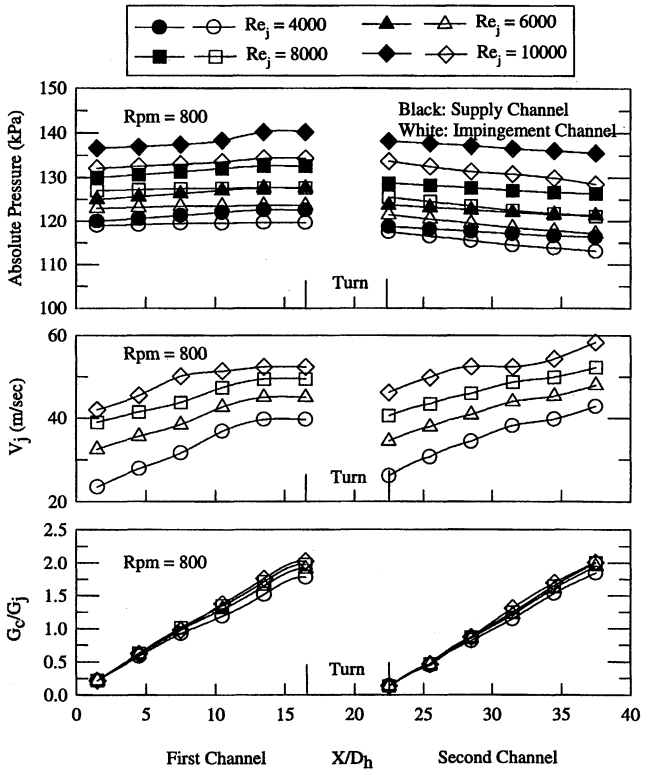

Fig. 4 Flow distribution for rotating test.

flux-to-jet flow mass flux also increased from the inlet to the exit of the channels. The jet velocity distributions in both channels were similar. The channel crossflow mass flux at a given radial location is the sum of all impinging jet mass fluxes upstream of that radial location.

Figure 4 shows the pressure distribution in the supply and impingement channels, the jet velocity distribution, and the distribution of the ratio of channel crossflow mass flux-to-jet flow mass flux for the rotating test (800 rpm, forward rotation). Rotation-induced centrifugal forces ($\rho\Omega^2 r$) created additional pressure forces in the supply and impingement channels. Therefore, higher pressures were recorded in the test model compared with the nonrotating test.

In the first channel, impinging jets traveled opposite to the direction of rotation. $\rho\Omega^2 r$ acted radially outward and pushed the air toward the exit of the channel. As expected, the jet velocities and the ratios of channel crossflow mass flux-to-jet flow mass flux increased in the radially outward direction. The values of the jet velocities and ratios of channel crossflow mass flux-to-jet flow mass flux are similar to those for the nonrotating test.

In the second channel, impinging jets traveled in the same direction of rotation. $\rho\Omega^2 r$ acted radially outward and opposed inertial motion of air in the supply and impingement channels. This caused a higher resistance to the air in the channel at large radial locations. Decreasing pressures were measured in the supply and impingement channels from the inlet to the exit of the channel. The jet velocities and the ratios of channel crossflow mass flux-to-jet flow mass flux increased in the radially inward direction. The values of the jet velocities and ratios of channel crossflow mass flux-to-jet flow mass flux are similar to those for the nonrotating test. The rotation changed the pressure distribution in both the supply and impingement channels; however, the values of the pressure difference across the jet plate, jet velocities, and ratios of channel crossflow mass flux-to-jet flow mass flux are not significantly altered.

Figure 5 shows the conceptual (conjectured) view of the flow and force distribution in the test model for the rotating

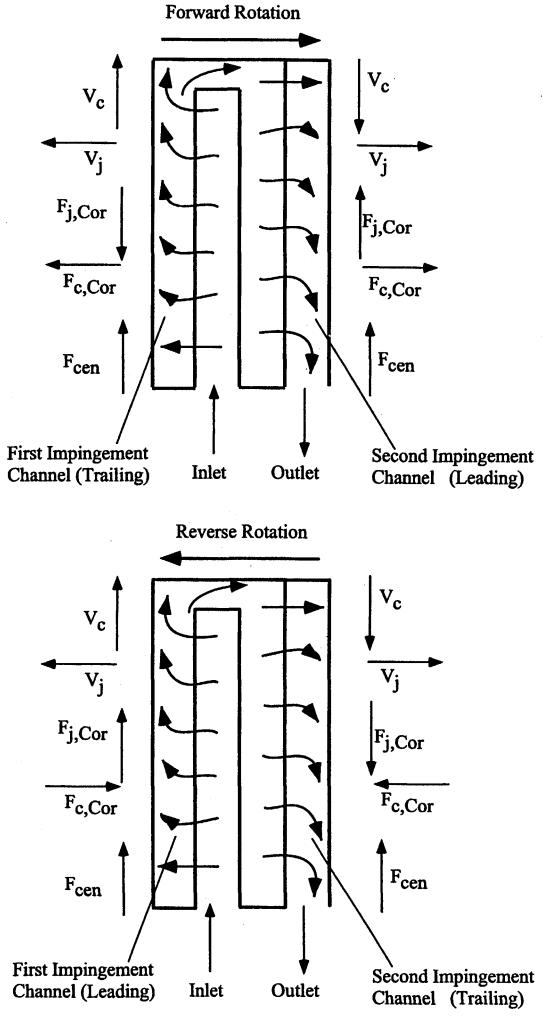

Fig. 5 Conceptual view of flow and force distribution.

tests (forward and reverse rotation). It is conjectured that the bending and deflection of jets would result in a lower impingement effect on the target walls. Therefore, lower heat transfer values were recorded during rotation compared with the values obtained from the nonrotating tests (Figs. 6 and 7).

Forward Rotation

In the first impingement channel, the jets traveled opposite to the direction of rotation. The magnitude of V_c increased in the radially outward direction, resulting in the bending of jets and lowered impingement effect on target walls. The channel Coriolis force, $\rho\Omega V_c$, pushed the cooler air toward the target wall and created higher velocity gradients near the target walls, which enhanced the heat transfer effect. Progressing from the inlet to the exit of the channel, the magnitude of the channel Coriolis force increased from 0 to 1045 g (for $Re_j = 1 \times 10^4$ and 800 rpm). The jet Coriolis force, $\rho\Omega V_j$, acted radially inward, resulting in the bending of jets and lowered impingement effect on target walls. Marching from the inlet to the exit of the channel, the magnitude of jet Coriolis force increased from 184 to 804 g (for $Re_j = 1 \times 10^4$ and 800 rpm). Also, $\rho\Omega^2 r$ acted radially outward and contributed to the bending of jets and lowering the impingement effect on target walls. Progressing from the inlet to the exit of the channel, the magnitude of centrifugal forces increased from 348 to 545 g (for $Re_j = 1 \times 10^4$ and 800 rpm). A complicated three-dimensional accelerated flow and secondary flow in the turn region caused higher-velocity gradients and higher heat transfer near the end walls.

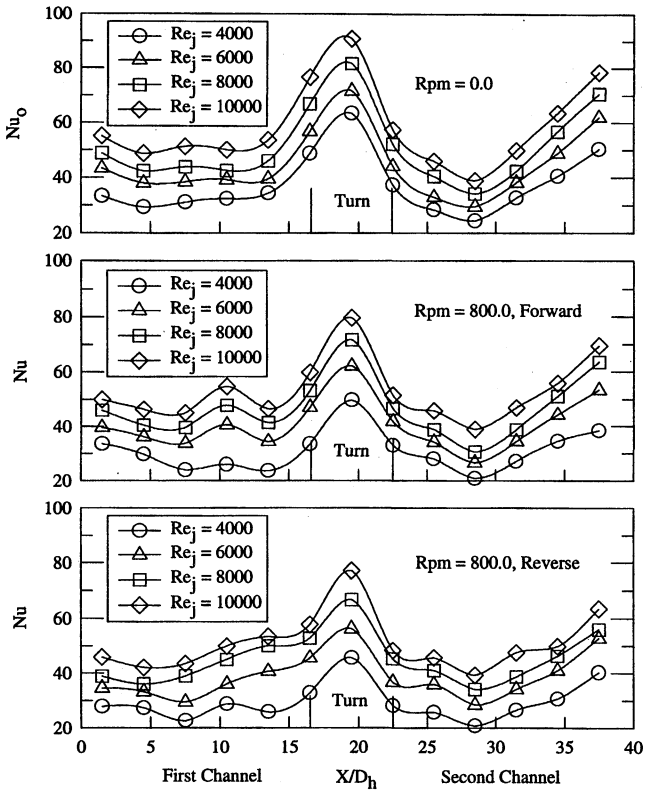

Fig. 6 Effect of Reynolds number on Nusselt number distribution.

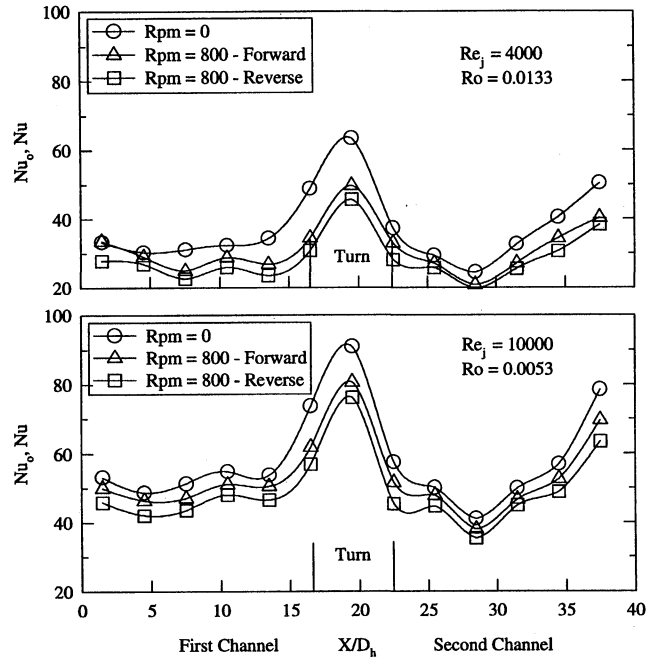

Fig. 7 Effect of rotation on Nusselt number distribution.

The jets traveled in the direction of rotation in the second impingement channel. The magnitude of V_c increased in the radially inward direction, resulting in the bending of jets and lowered impingement effect on target walls. $\rho\Omega V_c$ pushed cool air toward the target wall and created higher-velocity gradients near the target walls, which enhanced the heat transfer effect. $\rho\Omega V_j$ acted radially outward, resulting in the bending of jets and lowered impingement effect on the target walls. Also, $\rho\Omega^2 r$ acted radially outward and contributed to the bending of jets and lowering the impingement effect on target walls.

$\rho\Omega V_c$ pushed cooler air toward the target walls and enhanced impingement cooling effect in both impingement channels. However, $\rho\Omega V_j$ and $\rho\Omega^2 r$ caused the jets to bend and reduced the impingement effect on the target walls. These complicated flow and force distributions resulted in decreasing heat transfer coefficients for the forward rotation test compared with the nonrotation test (Figs. 6 and 7).

Reverse Rotation

In both impingement channels, $\rho\Omega V_c$ acted opposite to the jet velocity direction and pulled cooler air away from the target wall. This may have resulted in lower-velocity gradients near the target walls and a reduced impingement cooling effect. Meanwhile, $\rho\Omega V_j$ and $\rho\Omega^2 r$ caused the jets to bend and lowered the impingement effect on target walls. These complicated flow and force distributions resulted in lower-velocity gradients near the target walls compared with the forward rotation test. Therefore, lower heat transfer coefficients were recorded during the reverse rotation test compared with the forward rotation test (Figs. 6 and 7).

Figure 6 shows the regionally averaged Nusselt number distribution at various jet Reynolds numbers for the nonrotating and rotating tests. The Nusselt number is high at the stagnation point for a single jet impinging on the target wall. As the jet spreads on the target wall, velocity gradients near the target wall become small, resulting in the lower Nusselt number values.

Nonrotating Test

In the first impingement channel, the jet velocity and the channel crossflow mass flux increased in the radially outward direction, i.e., increasing X/D_h (Fig. 3). A higher channel crossflow deflects the jets away from the target wall and lowers the velocity gradients near the target wall. However, higher jet velocities penetrate the channel crossflow and impinge on the target wall. Higher jet velocities compensated for the degrading effect of the channel crossflow; therefore, relatively uniform Nusselt number values were observed for most of the channel. Upstream of the turn region, high jet and channel crossflow velocities produced large-velocity gradients near the target wall, and so high heat transfer values were recorded. Three-dimensional accelerated flow and secondary flow in the

turn region produced very high-velocity gradients; therefore, high Nusselt numbers were recorded in the turn region.

A sharp drop in Nusselt number values were observed, at the entrance in the second impingement channel. Lower heat transfer values were observed downstream of the entrance. Nusselt number values increased rapidly toward the exit of the channel. Jet velocities and channel crossflow mass flux increased from the inlet to the exit of the channel (Fig. 3). Jets with lower velocity at the entrance of the second channel produced lower Nusselt number values. Crossflow originating from the entrance region deflected the jets and lowered the impingement effect on the target wall; therefore, lower heat transfer values were recorded at the downstream locations of the entrance region. Near the exit of the channel, higher jet and channel crossflow velocities produced large velocity gradients near the target wall; therefore, high Nusselt number values were observed.

Rotating Test

The Nusselt number values were plotted for both forward and reverse rotation at various jet Reynolds numbers. Figures 4 and 5 show the nature of the flowfield and its influence on the heat transfer distribution for the rotation test. Figures 7 and 8 explain in detail heat transfer phenomena for the rotating test.

Figure 7 shows the effect of rotation on the Nusselt number distribution at two jet flow rates ($Re_j = 4 \times 10^3$ and 1×10^4) for both forward and reverse rotation ($\Omega = 800$ rpm). The trend showed that rotation did not significantly change Nusselt number distribution, but decreased Nusselt number values. Nusselt number values obtained with reverse rotation were lower when compared with those of the forward rotation values. This might be because of rotation-induced centrifugal and Coriolis forces, which cause the jets to bend and deflect away from the target walls. This would result in lower-velocity gradients near the target walls and reduce the impingement effect on target walls; therefore, lower Nusselt number values were obtained during the rotation test.

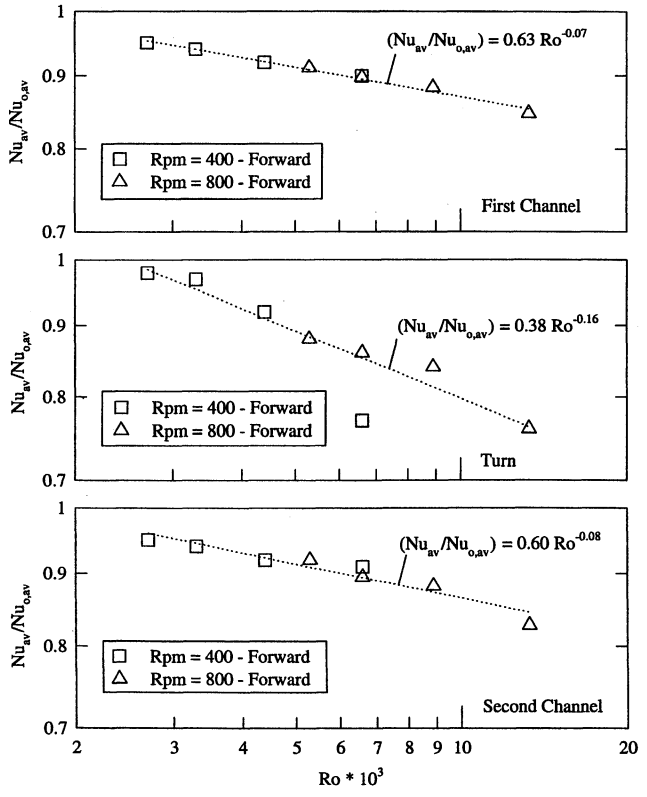

Fig. 8 Effect of rotation on channel-averaged Nusselt number ratio.

Figure 8 shows the channel-averaged Nusselt number ratios (ratio of rotation-to-nonrotation channel-averaged Nusselt numbers) at various rotation numbers ($\Omega d_j/V_{j,av}$). In this study, rotation numbers were varied in the 0.0–0.0133 range. At a fixed rotation speed, a lower jet Reynolds number gave a large rotation number and, likewise, a higher jet Reynolds number gave a low rotation number. Rotation decreased Nusselt number values 20 and 25% (below nonrotating values) in the impingement channels and the turn region, respectively. The Nusselt number ratios decreased with an increase in rotation numbers. A least-square curve fit was performed and correlations of the form $(Nu_{av}/Nu_{0,av}) = 0.63\ Ro^{-0.07}$, $(Nu_{av}/Nu_{0,av}) = 0.38\ Ro^{-0.16}$, and $(Nu_{av}/Nu_{0,av}) = 0.60\ Ro^{-0.08}$ were developed for the first impingement channel, the turn region, and the second impingement channel, respectively. The rotation number is an important parameter in correlating the Nusselt number values.

Figure 9 shows the channel-averaged Nusselt number values for various rotation speeds and jet Reynolds numbers. A least-square curve fit was performed for the nonrotating Nusselt number values, and correlations of the form $Nu_{0,av} = 0.63\ Re_j^{0.49}$ and $Nu_{0,av} = 2.35\ Re_j^{0.40}$ were developed for the impingement channels and the turn region, respectively. Reverse rotation decreased heat transfer values 22 and 28% in the impingement channels and the turn region, respectively, at $Re_j = 4 \times 10^3$. Reverse rotation also decreased heat transfer values 13% in the impingement channels and the turn region, at $Re_j = 1 \times 10^4$. The Nusselt number values in the turn region are about 60% higher when compared with the values in the impingement channels for higher flow rates over the range of rotation speeds tested.

Figure 10 compares the results obtained from current investigation (nonrotating test) with previous nonrotating studies. However, the investigations differed in geometric parameters and crossflow schemes. The Nusselt number values measured in this study followed the trends obtained from previous investigations. This study was conducted for maximum crossflow scheme and fixed geometric parameters, such as $d_j = 3.18$ mm, $X_n/d_j = 2$, $Y_n/d_j = 3$, $Z_n/d_j = 3$, and $A_f = 0.12$.

The heat transfer values measured in this study are 65, 35, 30, and 30% higher than Chance,[2] Parsons et al.,[8] Huang et al.,[5] and Kercher and Tabakoff,[1] respectively. Chance, Parsons et al., and Kercher and Tabakoff obtained results under a max-

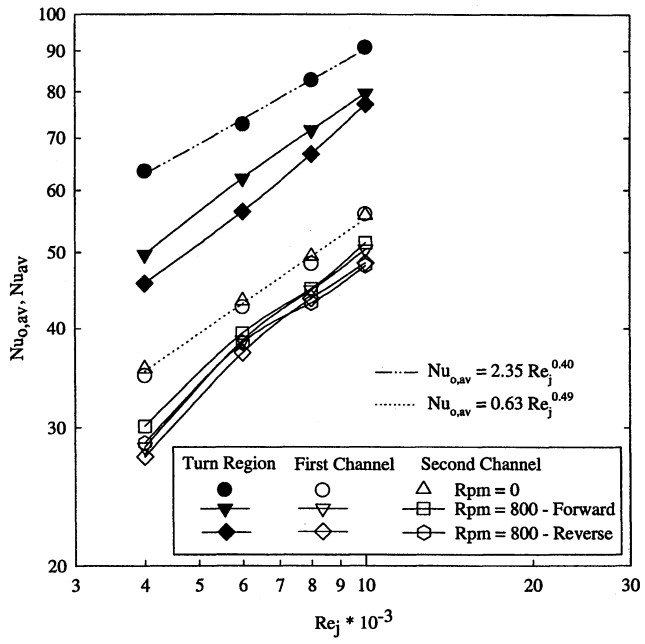

Fig. 9 Effect of Reynolds number on channel-averaged Nusselt number values at various rotation speeds.

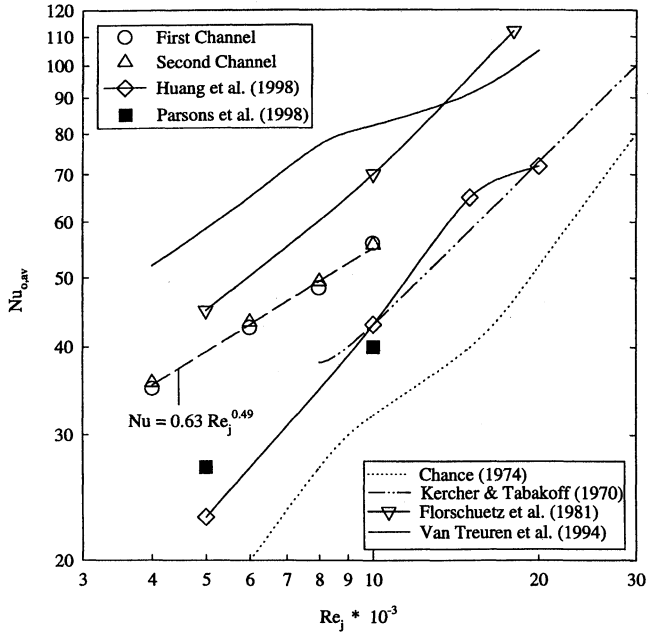

Fig. 10 Comparison of channel-averaged Nusselt number values with previous studies for nonrotating test.

imum crossflow scheme. The geometric parameters (d_j, X_n/d_j, Y_n/d_j, Z_n/d_j, and A_f) for Chance, Parsons et al., and Kercher and Tabakoff were 3.18 mm, 5, 5, 4, and 0.0276; 1.59 mm, 5, 5, 4, and 0.027; and 2.01 mm, 6.25, 6.25, 1, and 0.0201, respectively. Huang et al. reported local heat transfer values under various crossflow schemes, while the geometric parameters for this study were: d_j = 6.35 mm, X_n/d_j = 4, Y_n/d_j = 4, Z_n/d_j = 3, and A_f = 0.0491. The present study used more impingement cooling spots on the target walls, A_f, than Chance, Parsons et al., Huang et al., and Kercher and Tabakoff, which resulted in higher-velocity gradients and high Nusselt number values on the target walls. However, heat transfer values from this study are about 30 and 20% lower when compared with Van Treuren et al.[4] and Florschuetz et al.,[3] respectively. Both studies were performed under a minimum crossflow scheme. Van Treuren et al. presented local heat transfer measurements for the following geometric parameters: d_j = 5.08 mm, X_n/d_j = 8, Y_n/d_j = 8, and Z_n/d_j = 1. Florschuetz et al. presented correlations with different coefficients for in-line and staggered rows of jets. They presented a correlation for jet impingement with minimum crossflow, as well as a correlation with developing crossflow.

Conclusions

This study presented flow and heat transfer measurements from an in-line array of circular airjets in the midchord region of a simulated rotating gas turbine blade. Tests were performed in a two-pass rectangular impingement channel connected by a sharp 180-deg turn. Measurements were obtained with the jets impinging in the direction of rotation and also impinging opposite to the direction of rotation, in both the first and second impingement channels. The main conclusions are as follows.

1) Rotation increased the pressure level and changed the pressure distribution in the supply and impingement channels. However, the pressure drop across the jet plate and the jet velocity distribution in the two-pass impingement channel were not significantly altered by rotation.

2) Rotation-induced Coriolis and centrifugal forces deflected the jets away from the target walls. This resulted in a lower impingement effect and reduced the velocity gradients near the target walls. Therefore, lower heat transfer values were recorded during rotation.

3) Rotation decreased the Nusselt number values 20 and 25% below the nonrotating values in the impingement channels and the turn region, respectively.

4) Nusselt number values in the turn region were 60% higher when compared with the values in the impingement channels for higher jet flow rates over the range of rotation speeds tested.

5) Nusselt number ratios decreased with an increase in rotation numbers.

Acknowledgments

This paper was prepared with the support of the U.S. Department of Energy, Morgantown Energy Technology Center, Cooperative Agreement DE-FC21-92MC9061. The project was also supported by the Texas Higher Education Coordinating Board—Advanced Technology Program under Grant 999903-165 (TEES 32190-71720 ME). Their support is greatly appreciated.

References

[1]Kercher, D. M., and Tabakoff, W., "Heat Transfer by a Square Array of Round Air Jets Impinging Perpendicular to a Flat Surface Including the Effect of Spent Air," *Journal of Engineering for Power*, Vol. 92, No. 1, 1970, pp. 73–82.

[2]Chance, J. L., "Experimental Investigation of Air Impingement Heat Transfer Under an Array of Round Jets," *TAPPI*, Vol. 57, No. 6, 1974, pp. 108–112.

[3]Florschuetz, L. W., Truman, C. R., and Metzger, D. E., "Streamwise Flow and Heat Transfer Distributions for Jet Array Impingement with Cross Flow," *Journal of Heat Transfer*, Vol. 103, No. 2, 1981, pp. 337–342.

[4]Van Treuren, K. W., Wang, Z., Ireland, P. T., and Jones, T. V., "Detailed Measurements of Local Heat Transfer Coefficient and Adiabatic Wall Temperature Beneath an Array of Impinging Jets," *Journal of Turbomachinery*, Vol. 116, No. 2, 1994, pp. 369–374.

[5]Huang, Y., Ekkad, S., and Han, J. C., "Detailed Heat Transfer Distribution Under an Array of Orthogonally Impinging Jets," *Journal of Thermophysics and Heat Transfer*, Vol. 12, No. 1, 1998, pp. 73–79.

[6]Epstein, A. H., Kerrebrock, J. L., Koo, J. J., and Preiser, U. Z., "Rotational Effects on Impingement Cooling," Massachusetts Inst. of Technology, Gas Turbine Lab., Rept. 184, Cambridge, MA, Sept. 1985.

[7]Mattern, C., and Hennecke, D. K., "The Influence of Rotation on Impingement Cooling," *TurboExpo* (Birmingham, England, UK), ASME, New York (Paper 96-GT-161).

[8]Parsons, J. A., Han, J. C., and Lee, C. P., "Rotation Effect on Jet Impingement Heat Transfer in Smooth Rectangular Channels with Four Heated Walls and Radially Outward Cross Flow," *Journal of Turbomachinery*, Vol. 120, No. 1, 1998, pp. 79–85.

[9]Kline, S. J., and McClintock, F. A., "Describing Uncertainties in Single-Sample Experiments," *Mechanical Engineering*, Vol. 75, No. 1, 1953, pp. 3–8.